Desalination and Water Treatment
www.deswater.com
doi: 10.5004/dwt.2019.24262

158 (2019) 187–198
August

Lead and copper scavenging from aqueous solutions using *Eucalyptus camaldulensis* derived activated carbon: equilibrium, kinetics and sorption mechanism

M. Shafiq[a,*], A.A. Alazba[a,b], M.T. Amin[a,c]

[a]*Alamoudi Water Research Chair, King Saud University, Riyadh, Saudi Arabia, Tel. +966114673737; Fax: +966114673739; email: msrana@ksu.edu.sa (M. Shafiq)*
[b]*Agricultural Engineering Department, King Saud University, Riyadh, Saudi Arabia*
[c]*Department of Environmental Sciences, COMSATS Institute of Information Technology, Abbottabad, 22060, Pakistan*

Received 7 November 2018; Accepted 13 April 2019

ABSTRACT

In this study, activated carbon was derived from *Eucalyptus camaldulensis* (Ec_{activ}), activated though thermochemical (phosphoric acid) treatments and investigated for its efficiency to remove lead (Pb^{2+}) and copper (Cu^{2+}) from aqueous solutions. The contact time for equilibrium adsorption was estimated to be about 30 min, with a higher removal efficiency of Pb^{2+} compared to Cu^{2+} with insignificant removal after 2 h of contact time until 12 h, suggesting no adsorption within 2–12 h. The metal uptake and removal efficiency was almost two fold for Cu^{2+} while an even greater difference was seen for Pb^{2+} when the pH was varied from 2.5 to 5.5. A dose of 1.0 g of Ec_{activ} was deemed to be optimum for the highest uptake in the case of Pb^{2+} while for Cu^{2+}, the removal efficiency increased linearly with the increase in the dose of Ec_{activ} from 0.2 to 1.8 g. A 30% and 40% difference in the removal efficiency of Pb^{2+} and Cu^{2+}, respectively, was observed by increasing the initial solution concentration from 50 to 250 mg L^{-1} with an increase in the metal uptake of about 123 and 30 mg g^{-1} for Pb^{2+} and Cu^{2+}, respectively. Among the isotherm models, the Langmuir isotherm showed the best fit to the experimental data for both Pb^{2+} and Cu^{2+}, as confirmed by the respective high coefficients of determination. Finally, the kinetic behavior was best described by the pseudo-second-order model suggesting chemisorption of both heavy metal ions onto Ec_{activ}.

Keywords: Batch adsorption; Cu^{2+}; Langmuir isotherm; Process parameters; Pb^{2+}; Pseudo-second-order

1. Introduction

Rapid industrialization and urbanization has resulted in various environmental issues including the pollution of global water resources. Contamination of water resources due to heavy metals is of serious concern owing to the long-term persistency, toxicity, carcinogenicity, and non-biodegradability of the metals in the environment, plants and living organisms [1]. Among the most hazardous and frequently-occurring heavy metals, lead (Pb^{2+}) and copper (Cu^{2+}) are the most commonly occurring metals in the industrial wastewater released from the metal plating, paint, printing, constructions, mining, agrochemicals, and many other industries as well as from oil refineries [2–6]. Excessive amounts of the aforementioned metals are entering into the food chain on daily basis, causes severe health problems in animals and human beings such as brain hemorrhages, liver and kidney failures, paralysis, anemia and high blood pressure [7]. It is, therefore, devastating need of

* Corresponding author.

the time to limit the introduction of these heavy metals into water resources and to remove the prevailing metals from the waterbodies to ensure a safe and sustainable ecosystem.

Various chemical, biological and physical technologies have been employed by various researchers to eliminate the heavy metal contaminants from waste water such as membrane filtration, reverse osmosis, ion exchange, precipitation and adsorption or co-precipitation [8–14]. However, majority of these technologies require a tertiary treatment for the efficient removal of heavy metals from wastewater streams, which results in higher costs and inefficient remediation of the pollutants. Therefore, it has been established that adsorption through the use of adsorbent materials is a widely accepted, highly efficient and cost-effective remediation technique for the purification of water [15,16]. Whereas, the selection of an appropriate eco-friendly adsorbent with higher efficacy and lower operational cost is a critical factor to be considered. For instance, the application of activated carbon has attained a great deal of attention of researchers worldwide as an eco-friendly adsorbent with lower production cost, high purity, lower ash and high carbon contents [17,18]. It can be produced from carbonaceous or lignin-rich materials such as chestnuts [19], fruit stones [11,18], rice husks [20], coconut shells [21,22], rosemary plant waste [5], olive seed waste [23] and many others.

The properties of activated carbon primarily depend on the process of activation and the conditions applied during the activation process [24]. Chemical reagents, such as KOH, $ZnCl_2$ and H_3PO_4, have most commonly been used for the activation of carbons [25–27] to promote the decomposition of carbonaceous material, to increase the carbon yield and to inhibits the formation of tar [28]. Activated carbon prepared from sea-buckthorn stones using H_3PO_4 as activating agent is reported to have an adsorption capacity 51.81 mg g^{-1} for Pb^{2+} [29]. Likewise, activated carbon prepared from milk bush kernel shell using H_3PO_4 had 5.02 mg g^{-1} of adsorption capacity for Pb^{2+} [30]. Activated carbon of chestnut shell using H_3PO_4 had an adsorption capacity of 138.88 mg g^{-1} for Pb^{2+} [31]. Palm fruit epicarp derived activated carbon activated with H_3PO_4 exhibited an adsorption capacity of 58.62 mg g^{-1} for Pb^{2+} [32]. Similarly, activated carbon prepared from municipal organic waste using H_3PO_4 as activating agents was reported to possess an adsorption capacity for Pb^{2+} as 90 mg g^{-1} [16]. Activated carbon prepared from grape bagasse using H_3PO_4 had an adsorption capacity of 43.47mg g^{-1} for Cu^{2+} [33]. The reports suggested that the efficiency of the particular activated carbon is highly dependent on type of the feedstock and activation agents used. Therefore, scientists are in continuous surge to develop new activated carbon sources with higher efficiencies and lower costs.

The wood of *Eucalyptus camaldulensis* is very useful in manufacturing furniture and other household products, leaving huge amounts of sawdust waste, which consequently results in surface pollution. Recycling of eucalyptus sawdust to produce activated carbon may help reduce surface pollution on one hand, and water decontamination on the other. Therefore, we hypothesized that recycling of eucalyptus sawdust and synthesizing activated carbon using H_3PO_4 would serve as an efficient adsorbent for the removal of Pb^{2+} and Cu^{2+} from wastewater streams. To the best of our knowledge, no study has been published on the preparation of activated carbon from Eucalyptus sawdust waste with chemical activation using H_3PO_4 as activating agent. Hence, Eucalyptus sawdust was used as a precursor for the production of chemically activated carbon using H_3PO_4 as activating agent in this study. The efficacy of the produced adsorbent to adsorb Pb^{2+} and Cu^{2+} from aqueous solutions was investigated. Batch equilibrium and kinetics sorption experiments were conducted to study the effects of contact time, pH, adsorbent dose and initial metal ions concentrations on adsorption of Pb^{2+} and Cu^{2+} onto eucalyptus sawdust biomass-derived activated carbon. Various equilibrium and kinetic sorption models were employed to identify the operating sorption mechanism.

2. Materials and methods

2.1. Chemicals and reagents

Stock solutions of Pb^{2+} (1,000 mg L^{-1}) and Cu^{2+} (1,000 mg L^{-1}) were prepared by dissolving appropriate amounts of lead nitrate ($(Pb(NO_3)_2)$; Tianjin Benchmark Chemical Reagent Co. Ltd., Tianjin, China) and copper sulfate pentahydrate ($CuSO_4{\cdot}5H_2O$; AR grade Merck, Germany) in ultrapure water (Milli-Q integral water dispenser). The stock solutions were stored in 1 L volumetric flasks at 4°C for long-term use and preserved by the addition of 2 mL of concentrated HCl. Serial dilutions of the 1,000 mg L^{-1} stock solutions were prepared using distilled-deionized water to prepare the required initial concentrations of metal ions. The solution pH was also adjusted as desired in different batch experiments and 0.1 HCl and 0.1 M NaOH were used for this purpose while measuring the pH with a microprocessor-based pH meter (PHS-3CW, China).

2.2. Adsorbent preparation and characterization

Waste sawdust biomass of *Eucalyptus camaldulensis* (Ec) was collected from different locations in Riyadh, Kingdom of Saudi Arabia, and utilized as a precursor for the activated carbon preparation in a muffle furnace. Briefly, Ec waste was soaked in 1 M solution of phosphoric acid (H_3PO_4) at ratio of 1:7 (mixing 5 g waste biomass in 35 mL solution). The mixture was boiled at 80°C for 30 min [34]. After boiling, waste biomass was filtered out, washed with deionized water until neutral pH, and dried at 60°C for 6 h. Finally, the dried material was carbonized in a furnace (muffle) at 280°C for 170 min under an N_2 gas stream. The oxygen-free atmosphere was maintained until the carbonized material cooled down to 70°C. The produced material was stored in air-tight containers and labelled as Ec_{activ}.

American Society for Testing and Materials (ASTM) standard test methods were used to for the proximate analyses to measure the moisture, ash and volatile matte contents of both the Ec and Ec_{activ} while the ultimate analysis was performed using an element analyzer (Thermo Fisher Scientific, Berlin, Germany). To characterize the crystal structure and surface morphology of eucalyptus sawdust biomass-derived activated carbon, before and after adsorption of studies heavy metal ions, powder X-ray diffraction (XRD), Fourier-transform infrared (FTIR) with spectral range

between 4,000 and 600 cm^{-1}, and scanning electron microscopy (SEM) (VEGA3 SBU; TESCAN, USA) were performed.

2.3. Batch adsorption experiments

100 mL conical flasks were used for the batch experiments by shaking the samples for a specified time at 220 rpm and 30°C in a temperature-controlled Wise Cube orbital shaker (Daihan Scientific Co. Ltd, Wisd. ThermoStable IS-20, South Korea). Adsorption experiments were performed by selecting the appropriate amount of initial metal ions concentrations in the range 50–250 mg L^{-1} with a solution pH ranging from 2.5 to 5.5 and different amounts of Ec_{activ} were added in the range of 0.2–1.8 g. After shaking for a specific contact time (3, 5, 10, 15, 20, and 30 min and extended further to 1, 2, 3, 6, and 12 h), samples were withdrawn from the Shaker and were centrifuged at 1,000 rpm for 5 min in a centrifuge (Elektromag M815P model) to separate the adsorbate from the solution and filtered afterwards using a nitrocellulose filter paper (0.45 μm thick). The residual metal concentration in each sample was measured by flame atomic absorption spectrometry (FAAS, Thermo Scientific, ICE 3000 Series, Cambridge, United Kingdom).

The transient adsorption capacity, q_t (mg g^{-1}) at any contact time, t (min) is calculated by measuring the amount of adsorbed metal using FAAS. The equilibrium adsorption capacity, q_e (mg g^{-1}), and the removal efficiency (%) are calculated as:

$$q_e = \left(C_0 - C_e\right) \times \frac{V}{M} \tag{1}$$

$$\text{Removal}\left(\%\right) = \frac{\left(C_0 - C_e\right)}{C_0} \times 100 \tag{2}$$

where C_0 and C_e are the initial and equilibrium metal concentrations (mg L^{-1}) of the solution, respectively, and V and M are the volume of the solution (L) and the mass of dry adsorbent (g), respectively.

2.4. Equilibrium isotherms and kinetic models

The Langmuir, Freundlich, Temkin, Halsey, Harkin–Jura (H-J) and Dubinin–Radushkevich (D-R) isotherm models were used for further analysis of the batch experimental data to describe the adsorption capacity in relation to the residual adsorbate concentration. A pH of 5.5, contact time of 30 min, Ec_{activ} dose of 1.0 g, and initial metal concentration of 250 mg L^{-1} were employed to perform the analyses at 30°C. The rate of adsorption was evaluated by selecting different initial concentrations of both heavy-metal ions (50, 100, 150, 200, and 250 mg L^{-1}), as shown in Table 3, using pseudo-first-order and pseudo-second-order kinetic models. Constant process parameters included the solution pH and temperature of 5.5°C and 30°C, respectively, an adsorbent dose of Ec_{activ} of 1.0 g in addition to the variable time intervals in the range of 1 min to approximately 12 h.

3. Results and discussion

3.1. Characterization of Ec_{activ} before and after adsorption

A higher fixed carbon content (55.67 wt.%) was found in Ec_{activ} compared to the biomass of Ec (15.2 wt.%), as was indicated by the proximate analysis while volatile content in Ec_{activ} was almost half of the volatile content in Ec (60.23 wt.%). Furthermore, ultimate analysis revealed higher carbon content in Ec_{activ} compared with Ec (61.23 compared with 41.22 wt.%), confirming the yield of activated carbon from the used biomass of Ec in this study. Fig. 1a illustrates the XRD pattern of Ec sawdust chemically-activated carbon (Ec_{activ}) before and after lead (Ec_{activ}-Pb^{2+}) and copper (Ec_{activ}-Cu^{2+}) adsorption.

The XRD pattern of Ec_{activ} represented a typical diffraction pattern of an amorphous material with only one least-defined resolved broad peak at about 2θ = 25.63°. Similar diffraction pattern was noticed in previous studies [35]. A very sharp diffraction peak at 2θ = 30.18° after adsorption was identified as lead (PDF File No.: 230345) which suggested the adsorption of Pb^{2+} at the surface of Ec_{activ}. Similarly, a sharp diffraction peak at 2θ 43.93° was ascribed

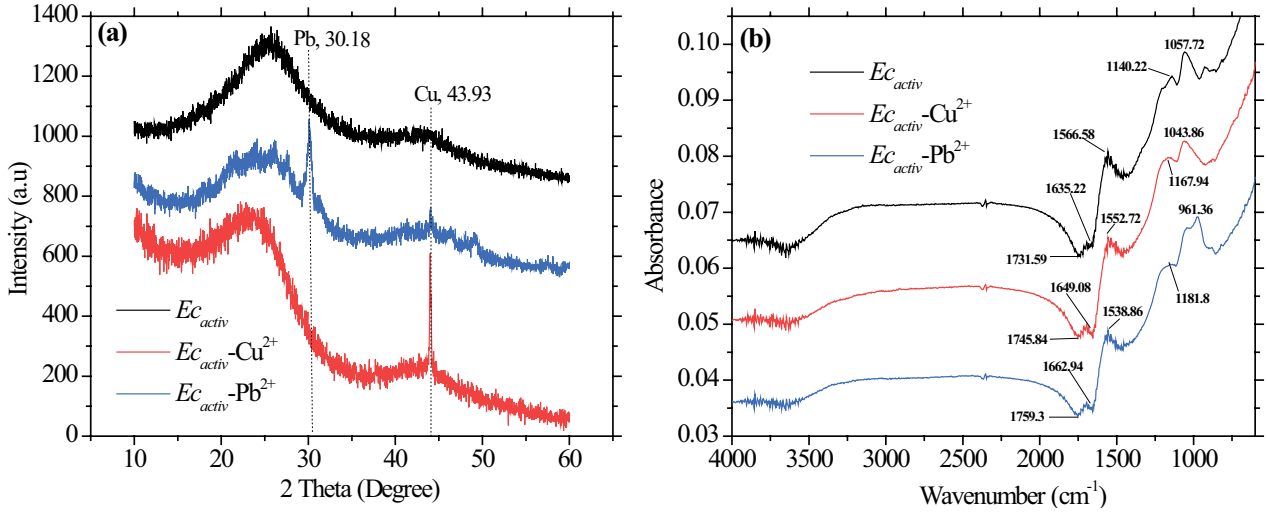

Fig. 1. (a) XRD pattern and (b) FTIR spectra of Ec_{activ} before and after lead adsorption (Ec_{activ}-Pb^{2+}), and copper adsorption (Ec_{activ}-Cu^{2+}).

to Cu^{2+} (PDF File No.: 03-1015, 85-1326, 04-0836) suggesting the adsorption of Cu^{2+} at the Ec_{activ} surface. These variations in the mineralogical phases of the adsorbent after metal adsorption confirm the interactions of metals at the surface of the sorbent materials.

The FTIR technique was employed to find the functional groups present on the surface of Ec_{activ} which were responsible for the adsorption of various contaminants from a polluted sample [36]. The FTIR spectra were recorded from 4,000 to 600 cm^{-1} (Bruker Alpha-Eco ATR-FTIR, Bruker Optics Inc, Germany) for Ec_{activ} before and after Pb^{2+} and Cu^{2+} ion sorption process as shown in Fig. 1b. Various bands at 1,731.59; 1,635.22; 1,566.58; 1,140.22; and 1,057.72 cm^{-1} were observed in Ec_{activ} spectrum prior to the sorption process. A band appearing at 1,731.59 cm^{-1} was ascribed as carbonyl (C=O) group, while a band at 1,635.22 cm^{-1} was designated as C=C groups. Likewise, a band at 1,566.58 cm^{-1} was ascribed as weak aromatic groups and the bands occurring at 1,140.22 and 1,057.72 cm^{-1} were ascribed as C–O group. It was noticed that many functional groups were shifted to different frequency levels after adsorption of the metals, indicating the possible involvement of those groups for adsorption of Pb^{2+} and Cu^{2+}. It can be seen that the peak around 1,057.72 cm^{-1} before adsorption was shifted to 961.36 and 1,043.86 cm^{-1} after the adsorption of Pb^{2+} and Cu^{2+}, respectively. A decrease in the intensities of the aforementioned peaks was observed suggesting a decrease in C–O group [37]. A peak around 1,566.58 cm^{-1} before adsorption was shifted to 1,538.86 and 1,552.72 cm^{-1} after adsorption of Pb^{2+} and Cu^{2+}, respectively. These peaks correspond to aromatic ring stretching in lignin [22,27]. A peak around 1,731.59 cm^{-1} before adsorption was shifted to 1,759.31 and 1,745.84 cm^{-1} after the adsorption of Pb^{2+} and Cu^{2+}, respectively. These peaks correspond to the stretching vibrations of the carbonyl group (C=O). The increment in the intensities of these aforementioned peaks indicated an anhydride modification which resulted in an increase in carbonyl groups present in ester bonds [37]. Hence, it is obvious that the surface functional groups of the adsorbent were acting as active sites for the efficient adsorption of Pb^{2+} and Cu^{2+} ions.

SEM images of Ec_{activ} before and after Pb^{2+} and Cu^{2+} adsorption is presented in Figs. 2a–c. Different types of irregular, narrow pore structures along with abundant long, cylindrical cavities can be seen in Ec_{activ} prior to adsorption (Fig. 2a). According to previous studies, it has been established that activation of Ec at 280°C with H_3PO_4 resulted in the creation of pores and cylindrical porous structures which changed the material surface properties and thus lead to higher adsorption capacities [38].

The macrographs after sorption in Fig. 2b and c clearly show the changes in surface morphology. Small metal particles of Pb^{2+} and Cu^{2+} can be seen on the surface of Ec_{activ}

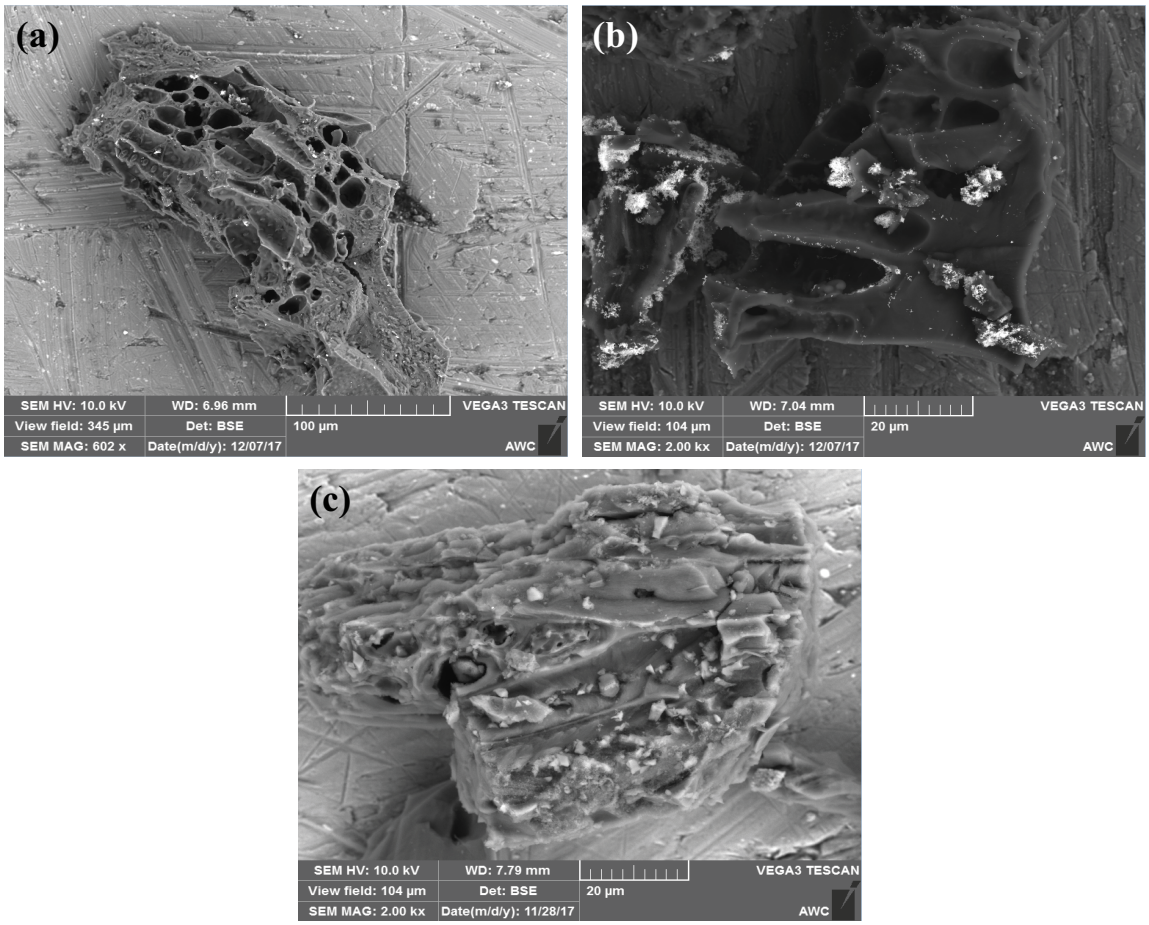

Fig. 2. Scanning electron microscopy images of Ec_{activ} (a) before and after (b) Pb^{2+}, and (c) Cu^{2+} adsorption.

confirming the successful adsorption process, which is in agreement with the XRD results. These findings suggest the occurrence of physiochemical interactions between the heavy-metal ions and functional groups present at the surface of Ec_{activ}, which have resulted in metal adsorption onto the surface of Ec_{activ}.

3.2. Effects of different process parameters on batch adsorption

Batch adsorption experiments were mostly performed in triplicate by taking 50 or 100 mL of metal solution in conical flasks. The appropriate amount of the adsorbent was used to achieve the desired dose of each batch test and the effects of the contact time, pH, initial metal concentration and adsorbent dose were investigated.

3.2.1. Effect of contact time

The efficiency of an adsorbent is determined by its contact time with the targeted contaminants [39,40]. Batch kinetic experiments at a pH value of 5.5 and initial metal concentrations of 100 mg L^{-1} were performed using the adsorbent dose of 1.0 g to determine the equilibrium time. The effect of contact time on the adsorption capacity and removal efficiency of both heavy-metal ions was analyzed at specific times of 3, 5, 10, 15, 20, and 30 min and further continued at 1, 2, 3, 6, and 12 h as shown in Fig. 3.

Significantly rapid adsorption and a high removal efficiency were observed for both heavy-metal ions during the first 10–20 min mainly owing to the presence of the uncovered surface area of the adsorbent [41]. Slower adsorption was then observed for approximately 15 min and the equilibrium time was attained at approximately 30 min, as shown in Fig. 3. A similar behavior of adsorption was seen for both heavy-metal ions; however, the metal uptake capacity and removal percentage for Pb^{2+} was higher than those for Cu^{2+}. Rest of batch parameters including solution pH, adsorbent dose and initial metal concentrations were optimized using an equilibrium time of 30 min.

3.2.2. Effect of solution pH

Batch experiments were also performed to determine the effects of pH on the adsorption capacity of Ec_{activ} for both

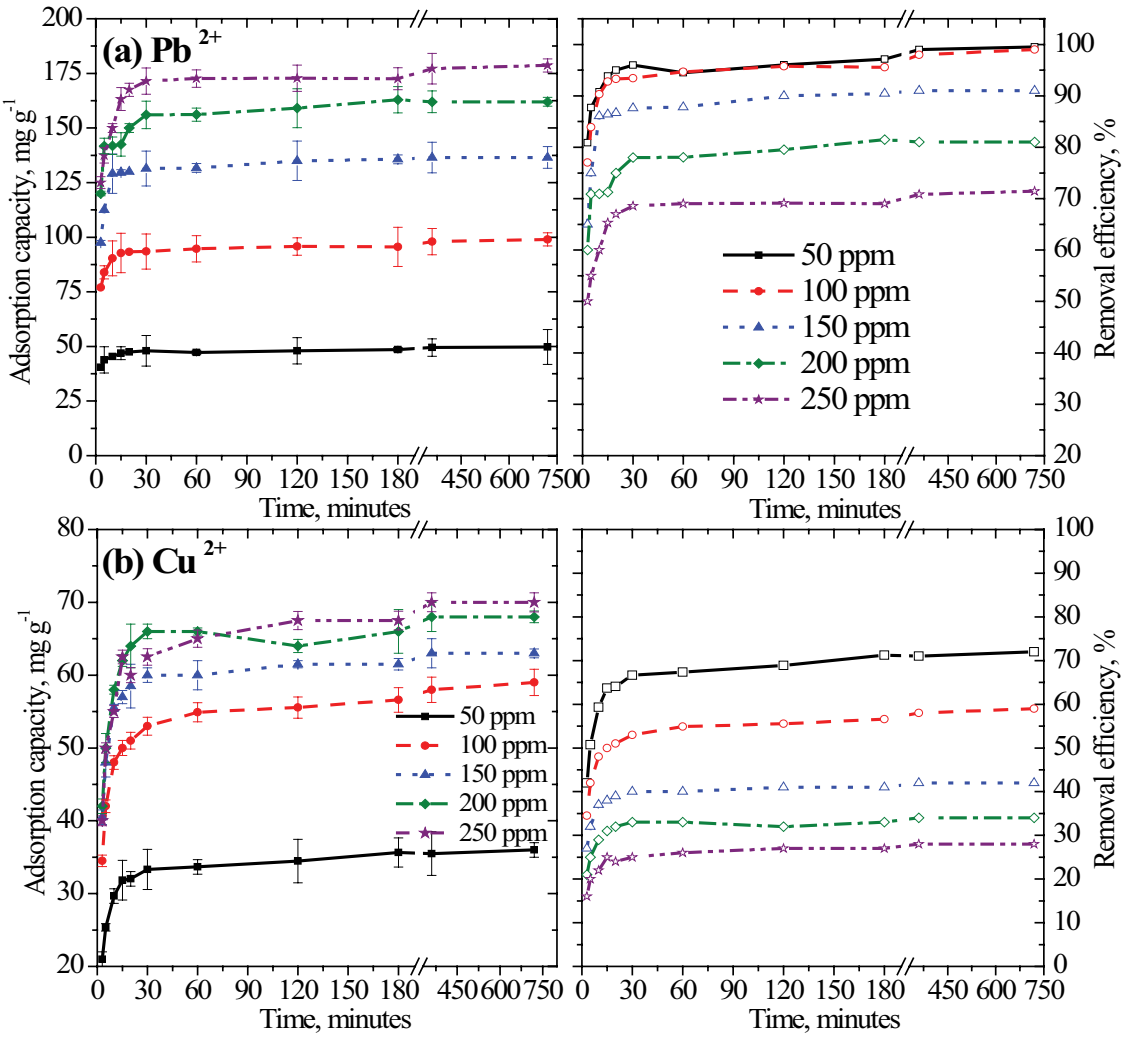

Fig. 3. Effects of contact time on adsorption capacity and removal efficiency of (a) Pb^{2+} and (b) Cu^{2+}.

Pb^{2+} and Cu^{2+}, as shown in Fig. 4. An adsorbent dose of 1.0 g was used for a contact time of 30 min with initial metal concentrations of 100 mg L^{-1} by varying the initial solution pH from 2.5 to 5.5.

As shown in Fig. 4, an increase in the removal efficiencies of both heavy-metal ions was seen by increasing the initial solution pH from 2.5 to 5.5 with optimum value around 5.0 for maximum adsorption capacity. Metal uptake was almost doubled for Cu^{2+} while even more difference was seen for Pb^{2+} by varying the pH from 2.5 to 5.5. The pH for the point of zero charge (pH_{ZPC}) of Ec_{activ}, as measured by titration with 0.1 M KNO_3 solution with initial pH range of 1.5–6, was estimate to be at 5.2. In this study, the maximum adsorption takes place at pH value of about 5.0 which is estimated to be about 90 and 50 mg g^{-1} for Pb^{2+} and Cu^{2+}, respectively. The effect of pH on the metal uptake efficiency of Ec_{activ} has demonstrated the changes in the surface charge and degree of ionization that govern the adsorption of heavy-metal ions [42,43]. At pH lower than pH_{ZPC}, i.e., 5.2 in this study, surface of Ec_{activ} acquire positive charge resulting an electrostatic repulsion between positively charged adsorbent and cationic metal ions. The presence of excess H^+ ions as a result of the acidic conditions (at a pH of 2.5) could be one of the reasons for the lowest metal uptake, as these ions compete with the divalent Pb^{2+} and Cu^{2+} ions for the adsorption sites on the surface of Ec_{activ} [44]. On the other hand, a high metal uptake at a pH of 5.5 compared to that at pH 2.5 could be due to the depressed electrostatic repulsion between the surface of the biochar, which is deprived of positive surface charge density, and the positively-charged metal ions [45].

3.2.3. Effect of adsorbent dose

The effect on the adsorption capacity of both heavy-metal ions and their removal percentage was studied using different initial concentrations of Ec_{activ} in the range of 0.2–1.8 g (Fig. 5). The other constant parameters of the batch experiments included the solution pH of 5.5, initial metal concentrations of 100 mg L^{-1} for both Pb^{2+} and Cu^{2+}, and the contact time of 30 min.

A linear increase of about 50%–60% in adsorption capacity and removal efficiency was seen by increasing the adsorbent dose from 0.2 to 1.8 g for both heavy-metal ions (Fig. 5). An

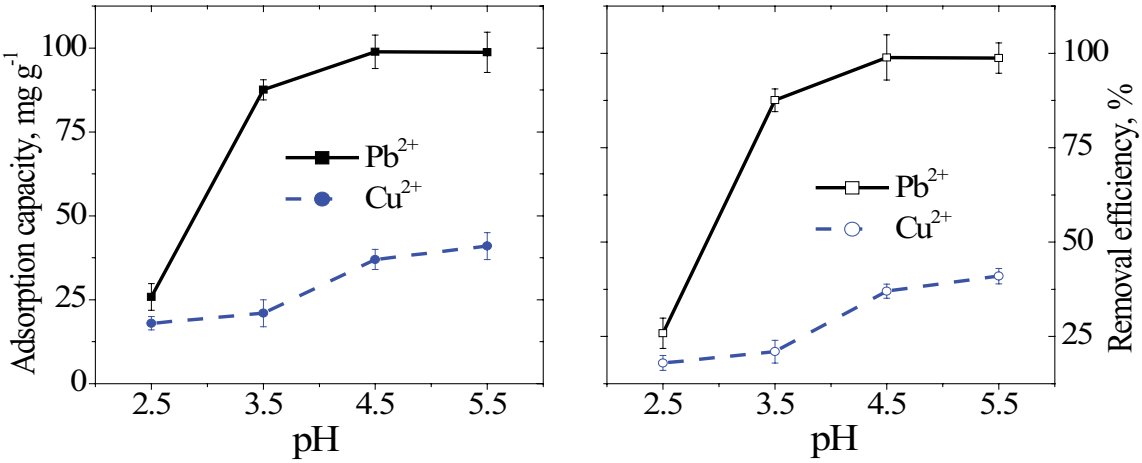

Fig. 4. Effects of solution pH on the adsorption capacity and removal efficiency of both heavy-metal ions.

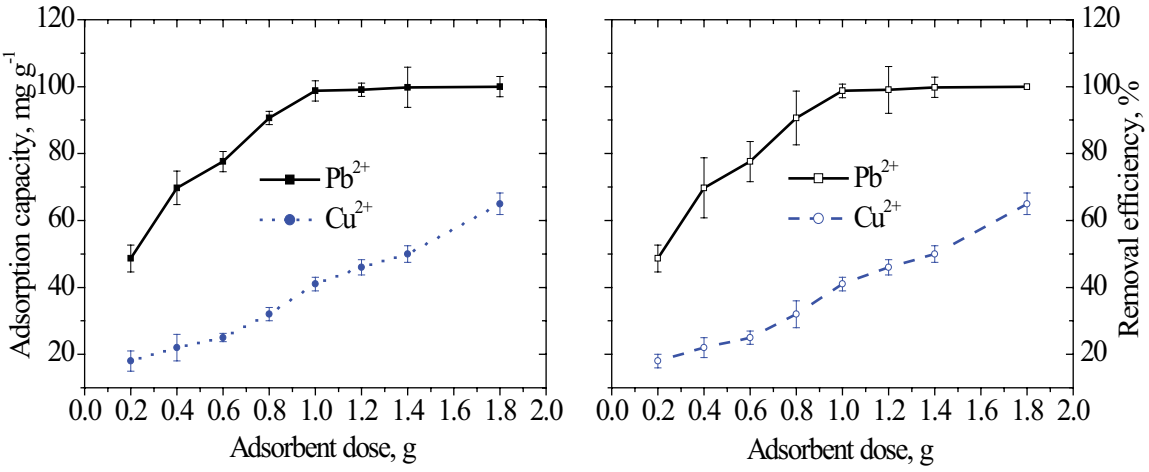

Fig. 5. Effects of adsorbent dose on metal adsorption capacity and removal efficiency of both heavy-metal ions.

Ec_{activ} dose of 1.0 g can be considered to be the optimum for highest uptake in the case of Pb^{2+} with insignificant changes from 1.0 to 1.8 g while for Cu^{2+}, removal efficiency continued to increase almost linearly until the maximum used dose of Ec_{activ} i.e., 1.8 g. This increasing trend of the metal uptake with the increasing dose of Ec_{activ} could be attributed to the availability of the active adsorption sites in large numbers, the greater surface area and the presence of abundant functional groups [46,47].

3.2.4. Effects of initial metal concentrations

Among the investigated parameters affecting the performance of batch adsorption, the effects of the initial metal concentrations were also examined using initial metal concentrations of both heavy-metal ions in the range 50–250 mg L^{-1} (Figs. 6a and b). The pH of the solution was kept constant at 5.5 during a contact time of 30 min while using 1.0 g of Ec_{activ}.

The removal efficiency of Pb^{2+} reduced to nearly 70% from 96% by increasing its initial solution concentration from 50 to 250 mg L^{-1} (Fig. 6a) while the difference in removal efficiency was about 40% for Cu^{2+} (Fig. 6b) for the same increase in the initial metal concentrations. However, an increased metal uptake of about 123 and 30 mg g^{-1} was observed for Pb^{2+} and Cu^{2+}, respectively, by increasing both of their initial solution concentrations from 50 to 250 mg L^{-1} thus attaining the optimum values around the maximum used concentration of 250 mg L^{-1}. A fairly high adsorption capacity and removal efficiency were observed for Pb^{2+} when compared with those of Cu^{2+} under similar adsorption conditions and pH values, contact time, Ec_{activ} dose and metal concentrations. At high initial concentrations of both heavy metal ions, concentration difference between heavy metal ions in the solution and that on the surface of Ec_{activ} is high which results in increased driving force and the maximum adsorption capacities of 171 and 63 mg g^{-1} were noticed when 250 mg L^{-1} of initial metal concentration was used. Furthermore, the saturation of adsorption sites and rapid filling or saturation of the binding sites on the surface of Ec_{activ}, might have caused decreased removal efficiency at high initial concentrations of both heavy-metal ions. As shown in Table 1, the maximum adsorption capacity of Ec_{activ} in this study is much high for Pb^{2+} when compared with previous studies that have used different adsorbents using same activation methods. For Cu^{2+}, however, some reported adsorbents have higher adsorption capacity than what was estimated using Ec_{activ} in this study.

3.3. Equilibrium isotherm models and adsorption kinetics

3.3.1. Isotherm models

The Langmuir model, assuming monolayer coverage, can be expressed in linear form as:

$$\frac{1}{q_e} = \frac{1}{q_{\max}} + \left(\frac{1}{q_{\max} K_{ads}}\right) \times \frac{1}{C_e} \tag{3}$$

where q_e and $q_{\max}$ (mg L^{-1}) are the equilibrium and maximum metal concentrations, respectively, C_e (mg L^{-1}) is the metal ion concentration in the solution, and K_{ads} (L mg^{-1}) is the Langmuir adsorption constant. The intercept and slope values of the plot $1/q_e \sim 1/C_e$ (Fig. 7a) relate to the $q_{\max}$ and K_{ads} values and the value of the coefficient of determination (R^2) of the linear fit is used to evaluate the fit to the equilibrium data. The value of R^2 close to unity (>0.99 as in Table 2) for both Pb^{2+} and Cu^{2+} shows the fitting of the adsorption data to the Langmuir isotherm (Table 2) which in turn describes the suitability of the Langmuir isotherm model for the adsorption of both heavy-metal ions on to Ec_{activ}. The predicted $q_{\max}$ was calculated as slightly higher than the experimental adsorption capacity reflecting the possibility of the saturation of Ec_{activ} at high initial metal concentrations (Table 2). The value of the Langmuir adsorption constant (K_{ads}) was much higher for Pb^{2+} (0.1914 L mg^{-1}) than Cu^{2+} (0.051 L mg^{-1}) in coincidental with the higher maximum adsorption capacity of Pb^{2+} compared with Cu^{2+} (172.4 compared with 73 mg g^{-1}), as shown in Table 2.

The adsorption of a heterogeneous system is well defined by the Freundlich isotherm model [48] that can be written in linear form as:

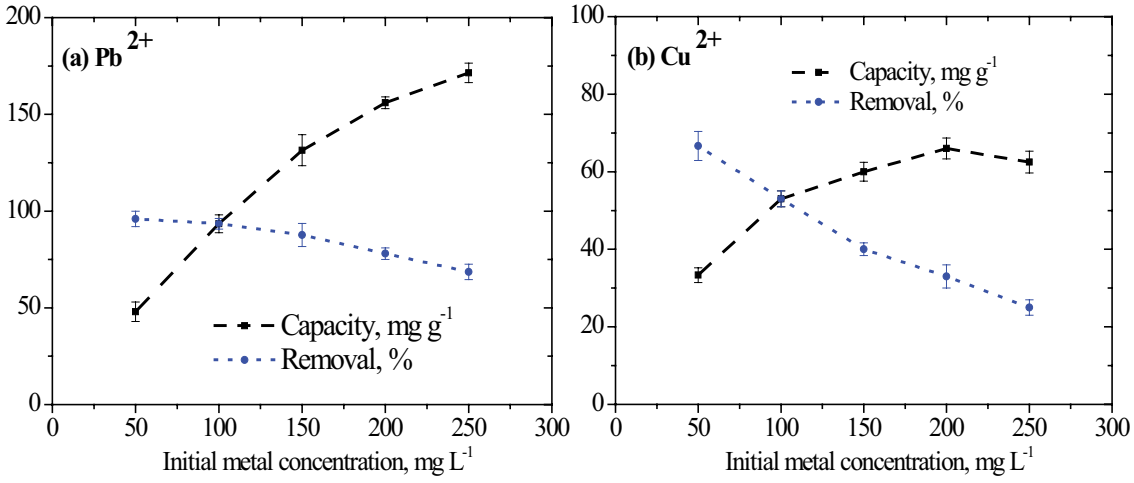

Fig. 6. Effects of initial metal concentration on the metal adsorption capacity of (a) Pb^{2+} and (b) Cu^{2+}.

Table 1
Comparison of adsorption capacity for Pb^{2+} and Cu^{2+} with previous studies

Adsorbent type	Contaminant	Maximum adsorption capacity, mg g^{-1}	Reference
Maize tassel based activated carbon	Pb^{2+}	37.31	[36]
Date bead activated carbon	Pb^{2+}	76.92	[51]
Activated date pits adsorbent	Cu^{2+}	33.44	[52]
African palm fruit activated carbon	Pb^{2+}	2.62	[53]
African palm fruit activated carbon	Cu^{2+}	1.52	[53]
Hazelnut shells activated carbon	Cu^{2+}	88.9	[54]
Grape bagasse activated carbon	Cu^{2+}	43.47	[33]
Activated carbon thorough micro-nano spheres	Pb^{2+}	46	[55]
Activated carbon thorough micro-nano spheres	Cu^{2+}	42	[55]
Cotton stalk activated carbon	Pb^{2+}	70.32	[56]
Pine cone activated carbon	Pb^{2+}	27.53	[57]
Van apple pulp	Pb^{2+}	17.7	[58]
Eucalyptus camaldulensis biomass activated carbon	Pb^{2+}	123	Current Study
	Cu^{2+}	30	

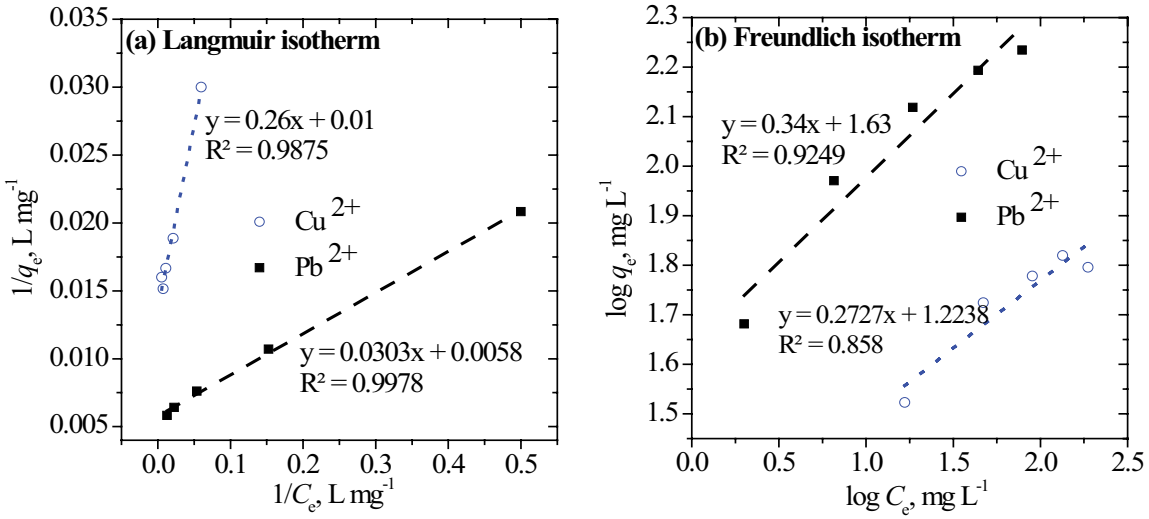

Fig. 7. The fitting of the experimental data to the (a) Langmuir and (b) Freundlich isotherm models for Pb^{2+} and Cu^{2+} biosorption.

$$\log q_e = \log K_F + \frac{1}{n}\log C_e \quad (4)$$

where q_e and C_e are described earlier, K_F (L g^{-1}) is the relative adsorption capacity, and $1/n$ is the dimensionless factor showing the adsorption intensity. Both K_F and $1/n$ are calculated from the intercept and slope of the linear plot ($\log q_e$ ~ $\log C_e$), as shown in Fig. 7b. The experimental fit of the equilibrium data in this isotherm model is evaluated from the R^2 value of the linear plot and is mentioned in Table 2.

The values of K_F were calculated as 39 and 15 L g^{-1} for Pb^{2+} and Cu^{2+}, respectively, while the respective n values calculated from the $1/n$ values in Table 2 are estimated as 2.94 and 3.67 showing the favorable adsorption of both heavy-metal ions onto Ec_{activ} since n lies in the range of 2–10. However, the lower values of R^2 (0.9249 and 0.858 for Pb^{2+} and Cu^{2+}, respectively) compared to those from the Langmuir isotherm model show that the equilibrium data for the adsorption of both heavy-metal ions are not in better agreement with the Freundlich isotherm model.

The linear form of the Temkin isotherm model is shown in Eq. (5a) and this model assumes a uniform distribution of binding energies on the surface of the adsorbent to cover the adsorbate-adsorbent interaction [49,50].

$$q_e = B_T \ln A_T + B_T \ln C_e \quad (5a)$$

$$B_T = \frac{RT}{b_T} \quad (5b)$$

where A_T (L g^{-1}) is the Temkin isotherm equilibrium binding constant calculated using the intercept value of the plot with q_e ~ ln C_e and B_T, which is the slope of the same plot. The

Table 2
Parameters of different isotherm models for the adsorption of Pb^{2+} and Cu^{2+} on to eucalyptus sawdust biomass-derived activated carbon

Isotherm	Parameter	Pb^{2+}	Cu^{2+}
Langmuir	$q_{e,exp}$, mg g^{-1}	171.469	62.5
	q_{max}, mg g^{-1}	172.4138	72.99
	K_{ads}, L mg^{-1}	0.1914	0.051
	R^2	0.9984	0.9907
Freundlich	K_F, L g^{-1}	38.876	15
	N	2.94	3.67
	R^2	0.9437	0.8935
Temkin	A_T, L mg^{-1}	2.286	1.0264
	b_T, kJ mol^{-1}	74.62	194.1
	R^2	0.9946	0.9195
Halsey	$q_{e,cal}$, mg g^{-1}	191.03	69.73
	n_H	–2.94	–3.668
	k_H	11.08	10.337
	R^2	0.9437	0.8935
Harkin-Jura	A, mg g^{-1}	5,000	1,666.67
	B	2	2.5
	R^2	0.7594	0.8316
Dubinin-Radushkevich	q_s, mol g^{-1}	162.65	69.28
	K, (mol $kJ^{-1})^2$	0.0006	0.0025
	E, kJ mol^{-1}	14.43	7.07
	R^2	0.9756	0.989

temperature, T (Kelvin) and the universal gas constant, R (8.314 J mol^{-1} K^{-1}) are used to calculate the value of b_T (kJ mol^{-1}), which is the Temkin isotherm constant, as shown in Table 2. Based on the value of R^2 (0.99 and 0.92 for Pb^{2+} and Cu^{2+}, respectively), the Temkin isotherm model seems to offer a good fit to the equilibrium data along with the Langmuir and Freundlich isotherm models. Ec_{activ} expressed higher maximum binding energy (A_T) for Pb^{2+} (2.29 L g^{-1}) than Cu^{2+} (1.03 L g^{-1}) while higher heat of adsorption (b_T) was seen for Cu^{2+} (194.1 kJ mol^{-1}) in comparison to Pb^{2+} (74.62 kJ mol^{-1}). The Halsey isotherm model is expressed in linear form as:

$$\ln q_e = \frac{1}{n_H}\ln k_H - \frac{1}{n_H}\ln C_e \tag{6}$$

where n_H and k_H are Halsey's isotherm constants and are calculated, respectively, from the slope and intercept of the plot with ln q_e ~ ln C_e. As indicated by the R^2 values (0.99 and 0.92 for Pb^{2+} and Cu^{2+}, respectively), a relatively poor fit of the Halsey isotherm model compared to that of Temkin and others confirms the homogeneous nature of the adsorbent. Similarly, a good fit of the equilibrium data is further reflected in slightly higher calculated values of q_e for both Pb^{2+} and Cu^{2+} (191 mg g^{-1} when compared with 171 mg g^{-1} for Pb^{2+}, and 70 mg g^{-1} when compared with 62 mg g^{-1} for Cu^{2+}), as shown in Table 2. Values of related non-linear parameters (n_H and k_H) in Halsey model were slightly higher for Pb^{2+} than Cu^{2+}, as shown in Table 2. The H-J isotherm model is written in the linear form as:

$$\frac{1}{q_e^2} = \frac{B}{A} - \left(\frac{1}{A}\right)\log C_e \tag{7}$$

where A and B are the H-J isotherm constants calculated from the slope and intercept values of the plot with $1/q_e^2$ ~ logC_e. A poor fit to the equilibrium adsorption data reflected by the low R^2 (0.76 and 0.83 for Pb^{2+} and Cu^{2+}, respectively), as shown in Table 2, may reflect that multilayer adsorption of the study's heavy-metal ions was not the case onto the surface of the Ec_{activ}. To distinguish between the physical and chemical adsorptions of metal ions, the D-R isotherm was applied and is expressed in the linearized form as:

$$\ln q_e = \ln q_s - K\varepsilon^2 \tag{8a}$$

$$\varepsilon = RT\ln\left(1+\frac{1}{C_e}\right) \tag{8b}$$

$$E = \frac{1}{\sqrt{2K}} \tag{8c}$$

where K is the D-R isotherm constant (mol^2 kJ^{-2}), q_s is the theoretical isotherm saturation capacity (mg g^{-1}), ε is the Polanyi potential, and E is the mean free energy of adsorption. Values of the intercept and slope of the plot with ln q_e ~ ε are used to calculate the q_s and K values, as shown in Table 2. A fairly significant value of R^2 for both heavy-metal ions (0.98 and 0.99 for Pb^{2+} and Cu^{2+}, respectively) confirms the suitability of this model for studies on the adsorption of heavy-metal ions on to the surface of Ec_{activ}. Finally, the E value of Pb^{2+} reflects the adsorption process as chemical (E = 8–16 kJ mol^{-1}) while physical adsorption is perceived for Cu^{2+} (E = 7.07 < 8 kJ mol^{-1}), as shown in Table 2.

3.3.2. Adsorption kinetics

Eqs. (9) and (10) present the linear form for both the pseudo-first-order and pseudo-second-order kinetic models, respectively.

$$\log\left(q_e - q_t\right) = \log q_e - \frac{k_1}{2.303}\times t \tag{9}$$

$$\frac{t}{q_t} = \frac{1}{k_2 q_e^2} + \frac{1}{q_e}\times t \tag{10}$$

where q_e and q_t are the amount of metal ions adsorbed per unit mass of adsorbent (mg g^{-1}) at equilibrium and at time t, respectively. The reaction rate constants, k_1 (h^{-1}) and k_2 (g mg^{-1} min^{-1}) for the pseudo-first-order and pseudo-second-order models, are calculated from the slope and intercept values of the plot with log (q_e – q_t) ~ t and t/q_t ~ t, respectively. As shown in Fig. 8, an excellent correlation with the

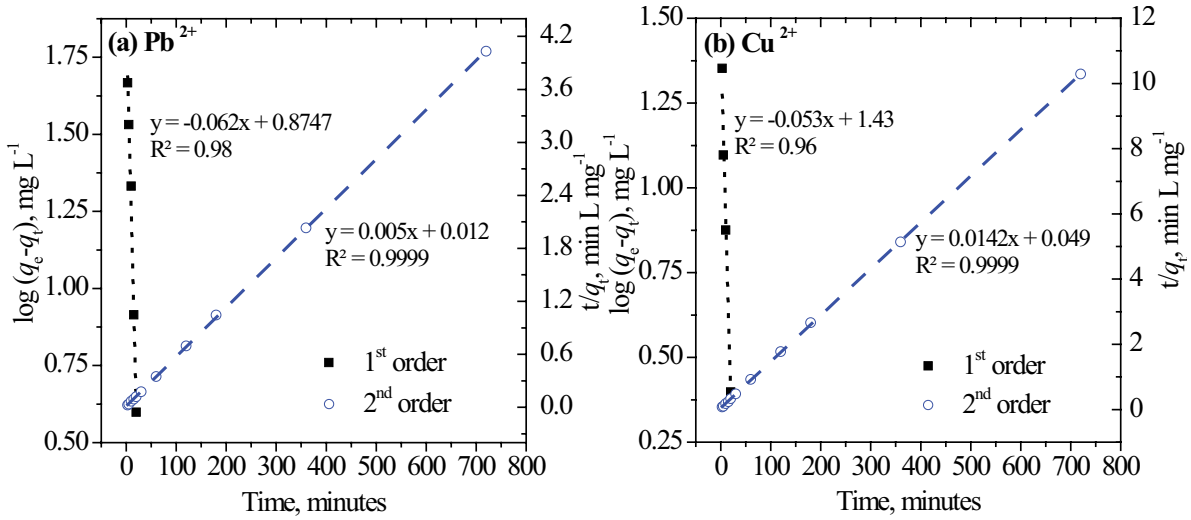

Fig. 8. Pseudo-first-order and pseudo-second-order kinetic plots with 250 mg L^{-1} initial solution concentration of (a) Pb^{2+} and (b) Cu^{2+}.

Table 3
Parameters of pseudo-second-order adsorption rate constants and calculated q_e at different initial concentrations of Pb^{2+} and Cu^{2+} on to eucalyptus sawdust biomass-derived activated carbon

Initial Pb^{2+} conc. (mg L^{-1})	$q_{e,exp}$ (mg g^{-1})	$q_{e,cal}$ (mg g^{-1})	k_2 (g mg^{-1} min^{-1})	h (mg g^{-1} min^{-1})	R^2
50	48	49.75	0.0109	27.1	1
100	93.449	99.01	0.0047	45.66	0.9999
150	131.463	136.986	0.0061	113.64	1
200	156	161.29	0.0045	116.28	1
250	171.469	178.57	0.0024	76.923	0.9999
Initial Cu^{2+} conc. (mg L^{-1})					
50	33.327	36.10	0.0094	12.24	1
100	53	59.17	0.0042	14.859	0.9999
150	60	63.29	0.0074	29.586	1
200	66	68.027	0.0059	27.25	0.9999
250	62.5	70.42	0.0041	20.28	0.9999

experimental data was observed for both heavy-metal ions by employing both pseudo-first-order and pseudo-second-order kinetic models (initial concentration of 250 mg L^{-1} for both Pb^{2+} and Cu^{2+}) as indicated by the high R^2 values (0.96–1), as shown in Figs. 8a and b.

Similarly, for other tested values of initial metal concentrations i.e., 100, 150, 200, and 250 mg L^{-1}, very high R^2 values (close to unity) were observed for both heavy-metal ions using the pseudo-second-order kinetic model, as shown in Table 3, displaying a linear relationship. The initial rate of adsorption (h in Table 3) was also calculated by taking the inverse of the intercept value in the plot with $t/q_t \sim t$ and is presented against each initial solution concentration of Pb^{2+} and Cu^{2+} in Table 3.

The pseudo-second-order model explains the kinetic behavior of the adsorption of Pb^{2+} and Cu^{2+} onto Ec_{activ} well as is reflected by the closeness of the calculated and the experimental adsorption capacities ($q_{e,cal}$ and $q_{e,exp}$ in Table 3). The good fit of the pseudo-second-order model helps considering the chemisorption to be the rate-controlling step for the adsorption of both heavy-metal ions on to the surface of Ec_{activ}.

4. Conclusions

In this study, the application of Ec_{activ} for the adsorption of Pb^{2+} and Cu^{2+} from aqueous media was investigated and SEM, XRD, and FTIR techniques were used to characterize the adsorbent. Different isotherm and kinetinc models were used to analyze the mechanism and behavior of the adsorption process. XRD patterns of Ec_{activ} indicated the presence of amorphous carbon, which reduced after lead and copper adsorption while FTIR spectra represented the shifting of many functional groups to different frequency levels after adsorption indicating the possible involvement of those groups for the adsorption of Pb^{2+} and Cu^{2+}. SEM images of Ec_{activ} before adsorption showed different types of irregular narrow pore structures along with abundant long cylindrical cavities which may lead to higher adsorption capacities.

Significant rapid adsorption during the first 15 min for Pb^{2+} and Cu^{2+} was followed by slower adsorption to reach equilibrium at about 30 min. A similar metal removal efficiency was observed for both heavy-metal ions with higher metal uptake of Pb^{2+} than that of Cu^{2+}. An increase in pH from 2.5 to 5.5 resulted in a two fold increase in the Cu^{2+} removal efficiency while even higher metal uptake was observed for Pb^{2+}. A 50%–60% increase in the adsorption capacity/removal efficiency by increasing the adsorbent dose from 0.2 to 1.8 g with 1.0 g of Ec_{activ} being the optimum dose for Pb^{2+}. An increase in metal uptake of about 123 and 30 mg g^{-1} for Pb^{2+} and Cu^{2+}, respectively, was seen by increasing the initial concentrations from 50 to 250 mg L^{-1}.

The Langmuir model agreed well with the experimental data for the adsorption of both heavy-metal ions based on the R^2 value. Other isotherm models exhibited the best-fit to the experimental data in the following order: Temkin > D-R > Halsey > Freundlich > H-J. The results indicated a good correlation with both kinetic models although the pseudo-second-order kinetic model better described the adsorption behavior of Pb^{2+} and Cu^{2+} onto Ec_{activ} and provided R^2 values close to 1.0, suggesting the chemisorptive nature of the investigated Ec_{activ}. The overall results demonstrated the effective absorption potential of Ec_{activ} for the studied heavy-metal ions and indicated the effectiveness of its use for potential applications in waste water treatment.

Acknowledgment

The project was financially supported by King Saud University, Vice Deanship of Research Chairs.

Conflict of Interest

Authors declare no conflict of interest.

References

[1] Q.-S. Liu, T. Zheng, P. Wang, J.-P. Jiang, N. Li, Adsorption isotherm, kinetic and mechanism studies of some substituted phenols on activated carbon fibers, Chem. Eng. J., 157 (2010) 348–356.
[2] M.A. Barakat, New trends in removing heavy metals from industrial wastewater, Arab. J. Chem., 4 (2011) 361–377.
[3] H.A. Hegazi, Removal of heavy metals from wastewater using agricultural and industrial wastes as adsorbents, HBRC J., 9 (2013) 276–282.
[4] M. Bilal, J.A. Shah, T. Ashfaq, S.M.H. Gardazi, A.A. Tahir, A. Pervez, H. Haroon, Q. Mahmood, Waste biomass adsorbents for copper removal from industrial wastewater—a review, J. Hazard. Mater., 263 (2013) 322–333.
[5] M.T. Amin, A.A. Alazba, M. Shafiq, Effective adsorption of methylene blue dye using activated carbon developed from the rosemary plant: isotherms and kinetic studies, Desal. Water Treat., 74 (2017) 336–345.
[6] M.T. Amin, A.A. Alazba, M. Shafiq, Removal of copper and lead using banana biochar in batch adsorption systems: isotherms and kinetic studies, Arab. J. Sci. Eng., 43 (2018) 5711–5722.
[7] P.B. Tchounwou, C.G. Yedjou, A.K. Patlolla, D.J. Sutton, Heavy Metals Toxicity and the Environment, EXS, 101 (2012) 133–164.
[8] N. Kongsricharoern, C. Polprasert, Electrochemical precipitation of chromium (Cr^{6+}) from an electroplating wastewater, Water Sci. Technol., 31 (1995) 109–117.
[9] L. Dai, L. Cui, D. Zhou, J. Huang, S. Yuan, Resource recovery of Cr(VI) from electroplating wastewater: laboratory and pilot-scale investigation using fibrous weak anion exchanger, J. Taiwan Inst. Chem. Eng., 54 (2015) 170–177.
[10] N. Tahir, H.N. Bhatti, M. Iqbal, S. Noreen, Biopolymers composites with peanut hull waste biomass and application for Crystal Violet adsorption, Int. J. Biol. Macromol., 94 (2017) 210–220.
[11] R. Mallampati, L. Xuanjun, A. Adin, S. Valiyaveettil, Fruit peels as efficient renewable adsorbents for removal of dissolved heavy metals and dyes from water, ACS Sustain. Chem. Eng., 3 (2015) 1117–1124.
[12] W.-P. Yang, Z.-J. Zhang, W. Deng, Simultaneous, sensitive and selective on-line chemiluminescence determination of Cr(III) and Cr(VI) by capillary electrophoresis, Anal. Chim. Acta, 485 (2003) 169–177.
[13] J. Yang, M. Yu, T. Qiu, Adsorption thermodynamics and kinetics of Cr(VI) on KIP210 resin, J. Ind. Eng. Chem., 20 (2014) 480–486.
[14] A. Kausar, H.N. Bhatti, M. Iqbal, A. Ashraf, Batch versus column modes for the adsorption of radioactive metal onto rice husk waste: conditions optimization through response surface methodology, Water Sci. Technol., 76 (2017) 1035–1043.
[15] B. Pan, B. Pan, W. Zhang, Q. Zhang, Q. Zhang, S. Zheng, Adsorptive removal of phenol from aqueous phase by using a porous acrylic ester polymer, J. Hazard. Mater., 157 (2008) 293–299.
[16] M.H. Al-Malack, A.A. Basaleh, Adsorption of heavy metals using activated carbon produced from municipal organic solid waste, Desal. Water Treat., 57 (2016) 24519–24531.
[17] N.K. Mandal, Performance of low-cost bio adsorbents for the removal of metal ions – a review, Int. J. Sci. Res., 3 (2014) 177–180.
[18] D. Prahas, Y. Kartika, N. Indraswati, S. Ismadji, Activated carbon from jackfruit peel waste by H_3PO_4 chemical activation: pore structure and surface chemistry characterization, Chem. Eng. J., 140 (2008) 32–42.
[19] V. Gómez-Serrano, E.M. Cuerda-Correa, M.C. Fernández-González, M.F. Alexandre-Franco, A. Macías-García, Preparation of activated carbons from chestnut wood by phosphoric acid-chemical activation. Study of microporosity and fractal dimension, Mater. Lett., 59 (2005) 846–853.
[20] S. Somasundaram, K. Sekar, V.K. Gupta, S. Ganesan, Synthesis and characterization of mesoporous activated carbon from rice husk for adsorption of glycine from alcohol-aqueous mixture, J. Mol. Liq., 177 (2013) 416–425.
[21] M.K.B. Gratuito, T. Panyathanmaporn, R.-A. Chumnanklang, N. Sirinuntawittaya, A. Dutta, Production of activated carbon from coconut shell: optimization using response surface methodology, Bioresour. Technol., 99 (2008) 4887–4895.
[22] Z. Hu, M.P. Srinivasan, Preparation of high-surface-area activated carbons from coconut shell, Microporous Mesoporous Mater., 27 (1999) 11–18.
[23] W.K. Lafi, Production of activated carbon from acorns and olive seeds, Biomass Bioenergy, 20 (2001) 57–62.
[24] G.G. Stavropoulos, A.A. Zabaniotou, Production and characterization of activated carbons from olive-seed waste residue, Microporous Mesoporous Mater., 82 (2005) 79–85.
[25] M. Song, Y. Wei, S. Cai, L. Yu, Z. Zhong, B. Jin, Study on adsorption properties and mechanism of Pb^{2+} with different carbon based adsorbents, Sci. Total Environ., 618 (2018) 1416–1422.
[26] I. Ozdemir, M. Şahin, R. Orhan, M. Erdem, Preparation and characterization of activated carbon from grape stalk by zinc chloride activation, Fuel Process. Technol., 125 (2014) 200–206.
[27] S. Yorgun, D. Yıldız, Preparation and characterization of activated carbons from Paulownia wood by chemical activation with H_3PO_4, J. Taiwan Inst. Chem. Eng., 53 (2015) 122–131.
[28] A. Kumar, H. Mohan Jena, High surface area microporous activated carbons prepared from fox nut (Euryale ferox) shell by zinc chloride activation, Appl. Surf. Sci., 356 (2015) 753–761.
[29] S.Z. Mohammadi, M.A. Karimi, D. Afzali, F. Mansouri, Removal of Pb(II) from aqueous solutions using activated carbon from Sea-buckthorn stones by chemical activation, Desalination, 262 (2010) 86–93.

[30] T.J. Afolabi, A.O. Alade, M.O. Jimoh, I.O. Fashola, Heavy metal ions adsorption from dairy industrial wastewater using activated carbon from milk bush kernel shell, Desal. Water Treat., 57 (2016) 14565–14577.
[31] H. Demiral, E. Baykul, M.D. Gezer, S. Erkoç, A. Engin, M.C. Baykul, Preparation and characterization of activated carbon from chestnut shell and its adsorption characteristics for lead, Sep. Sci. Technol., 49 (2014) 2711–2720.
[32] J.N. Ghogomu, S.N. Muluh, D.L. Ajifack, A.A.B. Alongamo, D.T. Noufame, Adsorption of lead (II) from aqueous solution using activated carbon prepared from raffia palm (Raphia Hookeri) fruit epicarp, J. Appl. Chem., 9 (2016) 74–85.
[33] H. Demiral, C. Güngör, Adsorption of copper(II) from aqueous solutions on activated carbon prepared from grape bagasse, J. Clean. Prod., 124 (2016) 103–113.
[34] M. Molina-Sabio, F. RodRíguez-Reinoso, F. Caturla, M.J. Sellés, Porosity in granular carbons activated with phosphoric acid, Carbon, 33 (1995) 1105–1113.
[35] M. Moyo, L. Chikazaza, B.C. Nyamunda, U. Guyo, Adsorption batch studies on the removal of Pb(II) using maize tassel based activated carbon, J. Chem., (2013) Article ID: 508934.
[36] M. Olivares-Marín, C. Fernández-González, A. Macías-García, V. Gómez-Serrano, Porous structure of activated carbon prepared from cherry stones by chemical activation with phosphoric acid, Energy Fuels, 21 (2007) 2942–2949.
[37] H. Ismail, H.P.S. Abdul Khalil, The effects of partial replacement of oil palm wood flour by silica and silane coupling agent on properties of natural rubber compounds, Polym. Test., 20 (2000) 33–41.
[38] H.P.S. Abdul Khalil, P. Firoozian, I.O. Bakare, H.M. Akil, A.M. Noor, Exploring biomass based carbon black as filler in epoxy composites: flexural and thermal properties, Mater. Des., 31 (2010) 3419–3425.
[39] Y.S. Ho, J.C.Y. Ng, G. McKay, Kinetics of pollutant sorption by biosorbents: review, Sep. Purif. Methods, 29 (2000) 189–232.
[40] K.A. Krishnan, T.S. Anirudhan, Removal of cadmium(II) from aqueous solutions by steam-activated sulphurised carbon prepared from sugar-cane bagasse pith: kinetics and equilibrium studies, Water SA, 29 (2003) 147–156.
[41] R. Qadeer, S. Akhtar, Kinetics study of lead ion adsorption on active carbon, Turk. J. Chem., 29 (2005) 95–100.
[42] M.A. Al-Ghouti, J. Li, Y. Salamh, N. Al-Laqtah, G. Walker, M.N.M. Ahmad, Adsorption mechanisms of removing heavy metals and dyes from aqueous solution using date pits solid adsorbent, J. Hazard. Mater., 176 (2010) 510–520.
[43] D.W. O'Connell, C. Birkinshaw, T.F. O'Dwyer, Heavy metal adsorbents prepared from the modification of cellulose: a review, Bioresour. Technol., 99 (2008) 6709–6724.
[44] M.A. Al-Ghouti, M.A.M. Khraisheh, S.J. Allen, M.N. Ahmad, The removal of dyes from textile wastewater: a study of the physical characteristics and adsorption mechanisms of diatomaceous earth, J. Environ. Manage., 69 (2003) 229–238.
[45] J.P. Chen, M. Lin, Equilibrium and kinetics of metal ion adsorption onto a commercial H-type granular activated carbon: experimental and modeling studies, Water Res., 35 (2001) 2385–2394.
[46] D. Uzunoğlu, N. Gürel, N. Özkaya, A. Özer, The single batch biosorption of copper(II) ions on Sargassum acinarum, Desal. Water Treat., 52 (2014) 1514–1523.
[47] A.E. Ofomaja, Y.-S. Ho, Equilibrium sorption of anionic dye from aqueous solution by palm kernel fibre as sorbent, Dyes Pigments, 74 (2007) 60–66.
[48] K. László, A. Bóta, L.G. Nagy, Comparative adsorption study on carbons from polymer precursors, Carbon, 38 (2000) 1965–1976.
[49] M.J. Temkin, V. Pyzhev, Kinetics of ammonia synthesis on promoted iron catalysts, Acta Physicochim URSS, 12 (1940) 217–222.
[50] P.S. Kumar, K. Ramakrishnan, R. Gayathri, Removal of nickel(II) from aqueous solutions by Ceralite IR 120 cationic exchange resins, J. Eng. Sci. Technol., 5 (2010) 232–243.
[51] M. Danish, R. Hashim, M. Rafatullah, O. Sulaiman, A. Ahmad, Adsorption of Pb(II) ions from aqueous solutions by date bead carbon activated with $ZnCl_2$, CLEAN – Soil Air Water, 39 (2011) 392–399.
[52] N.M. Hilal, I.A. Ahmed, R.E. El-Sayed, Activated and nonactivated date pits adsorbents for the removal of copper(II) and cadmium(II) from aqueous solutions, Int. Scholarly Res. Not., 2012 (2012) 1–11.
[53] S. Abdulrazak, K. Hussaini, H.M. Sani, Evaluation of removal efficiency of heavy metals by low-cost activated carbon prepared from African palm fruit, Appl. Water Sci., 7 (2017) 3151–3155.
[54] D.D. Milenković, M.M. Milosavljević, A.D. Marinković, V.R. Đokić, J.Z. Mitrović, A.L. Bojić, Removal of copper(II) ion from aqueous solution by high-porosity activated carbon, Water SA, 39 (2013) 515–522.
[55] F.-C. Huang, C.-K. Lee, Y.-L. Han, W.-C. Chao, H.-P. Chao, Preparation of activated carbon using micro-nano carbon spheres through chemical activation, J. Taiwan Inst. Chem. Eng., 45 (2014) 2805–2812.
[56] K. Li, Z. Zheng, Y. Li, Characterization and lead adsorption properties of activated carbons prepared from cotton stalk by one-step H_3PO_4 activation, J. Hazard. Mater., 181 (2010) 440–447.
[57] M. Momčilović, M. Purenović, A. Bojić, A. Zarubica, M. Ranđelović, Removal of lead(II) ions from aqueous solutions by adsorption onto pine cone activated carbon, Desalination, 276 (2011) 53–59.
[58] T. Depci, A.R. Kul, Y. Önal, Competitive adsorption of lead and zinc from aqueous solution on activated carbon prepared from Van apple pulp: study in single- and multi-solute systems, Chem. Eng. J., 200–202 (2012) 224–236.